Shear-induced phase behavior of bidisperse jammed suspensions of soft particles

Rakan Alrashdan,[1] Harry Kojo Yankah,[2] Michel Cloître,[3] and Fardin Khabaz*[1,2]

[1)]*School of Polymer Science and Polymer Engineering, The University of Akron, Akron, OH, 44325, United States.*

[2)]*Department of Chemical, Biomolecular, and Corrosion Engineering, The University of Akron, Akron, OH, 44325, United States.*

[3)]*Molecular, Macromolecular Chemistry, and Materials, ESPCI Paris, CNRS, PSL Research University, 75005 Paris, France.*

(*Electronic mail: fkhabaz@uakron.edu)

(Dated: 28 June 2024)

Particle dynamics simulations are used to determine the shear-induced microstructure and rheology of jammed suspensions of soft particles. These suspensions, known as soft particle glasses (SPGs), have an amorphous structure at rest but transform into ordered phases in strong shear flow when the particle size distribution is relatively monodisperse. Here, a series of bidisperse SPGs with different particle radii and number density ratios are considered, and their shear-induced phase diagrams are correlated with the macroscopic rheology at different shear rates and volume fractions. These shear-induced phase diagrams reveal that a combination of these parameters can lead to the emergence of various microstructures such as amorphous, layered, crystals, and in some cases, coexistence of amorphous and ordered phases. The evolution of the shear stress is correlated with the change in the microstructure and is a shear-activated process. Stress shows pseudo-steady behavior during an induction period before the final microstructural change leading to the formation of ordered structures. The outcomes provide a promising method to control the phase behavior of soft suspensions and build new self-assembled microstructures.

I. Introduction

Microstructure and macroscopic shear rheology of yield stress fluids, such as soft particle glasses (SPGs),[1,2] are determined by the volume fraction of particles ϕ, shear rate $\dot{\gamma}$, and particle size distribution.[3–8] SPGs, which are in the form of concentrated emulsions, microgels, star polymers with many arms,[2,9] consist of deformable particles that are jammed at volume fractions above the random close packing of equivalent hard-sphere suspensions (*i.e.*, $\phi_{rcp} = 0.64$).[10] In these suspensions, every particle is trapped in a cage formed by the first neighboring particles in contact. At contacts, particles exert elastic and lubrication forces onto one another. Unlike hard-sphere glasses, which solely encounter forces arising from excluded volume interactions, SPGs undergo compression through a bulk osmotic force and interact through an elastic repulsive potential.[5] Depending on the particle size distribution, they can form ordered structures in shear flow at volume fractions larger than ϕ_{rcp}.[6,7,11,12] SPGs behave like weak elastic solids at rest but flow macroscopically and exhibit shear thinning behavior under the application of stresses larger than a stress value known as the dynamic yield stress σ_y.[1,13] The shear rate dependence of the shear stress is often expressed by the Herschel-Bulkley (HB) equation, $\sigma = \sigma_y + k\dot{\gamma}^n$, where n is the exponent close to 0.50, k is the consistency parameter.[1,8,14]

It has been recognized that the distribution of particle sizes significantly influences the crystallization behavior of hard spheres.[15–18] Prior works have investigated the impact of polydispersity on the rheological properties and phase behavior of hard spheres.[19] In a quiescent state, suspensions with particle size distribution skewed towards smaller sizes transform into small crystallites that are not aligned or ordered in a consistent pattern across the material, resembling a smectic-like phase.[20,21] Suspensions with symmetrical and skewed size distribution towards large particles exhibit qualitatively distinct growth behaviors.[22] This observation implies a growth mechanism in which crystallization coincides with a local fractionation process near the crystal-fluid interface. The crystallization process in colloidal hard spheres proceeds through two distinct stages: precursor and induction stages.[23,24] These stages are marked by the growth of clusters with long-lived nonequilibrium structures, followed by a delayed nucleation process, respectively. The limited growth due to polydispersity is responsible for the induction stage and directly contributes to the delayed nucleation. Furthermore, experimental observations, using poly-methylmethacrylate, have shown that colloidal crystals of type AB_2 and AB_{13} in binary hard sphere suspensions are formed, and the stability of these crystals rely on the size ratios.[17,18]

Shear-induced phase behavior of soft colloids

In the case of hard spheres, the application of either oscillatory or steady shear influences the microstructure and rheology of colloidal suspensions, particularly comprised of sterically stabilized colloidal particles.[25–28] These hard particles can form shear-induced microstructures. Shear-induced ordering has been observed previously in volume fractions below the random close-packing fractions for hard spheres . In general, the phase behavior of Brownian soft particles below random-close packing at rest is similar to that seen in the hard sphere since the dominant interaction is based on thermal motion.[29–36] Both the structural and rheological characteristics of dense colloidal suspensions are influenced by factors such as the volume fraction of colloids, size distribution, inter-colloid interactions and the shearing conditions. Generally, in oscillatory shear flow, suspensions of hard spheres show different arrangements. FCC ordering is observed at low strain and frequency amplitudes, while hexagonally close-packed layers form at higher amplitudes.[6] Oscillatory shear flow can induce order-to-disorder transition.[37] These amorphous to crystalline transitions include crystalline formations such as face-centered cubic (FCC) structures, layers stacked in hexagonal patterns (HCP) between $\phi = 0.545$ and 0.58, as well as string, and liquid-like arrangements.[38,39]

Compared to hard spheres, the process of quiescent crystallization in dense suspensions of soft colloids is generally more complex, primarily due to particle shape fluctuations and volume adjustments.[21,40] The softness and spatial distribution of particles within the microstructure determine the macroscopic characteristics of these colloidal suspensions.[2,41,42] In quiescent conditions, a variety of structures can emerge, and their nature is based on the interplay of Brownian, repulsive, and attractive forces.[6,43] In the case of relatively monodisperse microgels, the initiation of fluid-crystal coexistence takes place at the identical volume fraction of 0.494, similar to hard spheres. Conversely, polydisperse microgels do not undergo crystallization but instead form an entropic glassy state, progressing further into a jammed glassy state.[44] When experimentally investigating poly(N-isopropylacrylamide) microgels, Scotti *et al.* observed a shift in the fluid-crystal transition to higher concentrations depending on the the polydispersity of the suspension.[45] It is important to note that even minor changes in the particles' surface roughness can significantly affect their interactions and phase behavior.[46] Thus, the phase behavior of concentrated suspensions depends on the volume fraction and the interaction at contact.

Similar to hard spheres, soft particles undergo microstructural changes when subjected to oscillatory or steady shear flows in experiments, and the response of spherical jammed suspensions undergoing shear deformation is characterized by out-of-equilibrium phase diagrams.[47–49] These

diagrams illustrate that above the freezing point, amorphous suspensions can transition into FCC structures, sliding layer configurations, or mixtures depending on the applied strain amplitude and frequency.[29] In oil-in-water emulsions subjected to large-amplitude shear oscillations, light scattering studies have revealed the induction of sliding hexagonal layers in the microstructure. The specific ordering observed is contingent upon the volume fraction and shear history of the sample, particularly near or above the jamming volume fraction.[50] Ultrasoft colloidal star polymers with a volume fraction close to the glass transition line exhibit a crystal-to-crystal transition under oscillatory shear flow. For instance, 1,4-polybutadiene stars undergo a direct transformation from a BCC-dominated phase to an HCP-like microstructure within an intermediate range of Péclet numbers.[51]

Similarly in simulations, utilization of either oscillatory or steady shear flows alters both the microscopic arrangement of colloidal soft suspensions and their rheological response.[52] In this regard, Khabaz *et al.*[6,7] studied the rheology of polydisperse soft particles with varying degrees of polydispersity undergoing both steady and oscillatory shear flows. The impact of steady shear and polydispersity on the rheological properties and microstructure of SPGs was explored. Jammed suspensions of soft particles, irrespective of their volume fractions, can undergo shear-induced ordering. The microstructure transforms from an amorphous phase to a layered structure aligned parallel to the flow-vorticity plane. The influence of particle geometry on these transformations, particularly for elongated particles, has been explored by Bearon and Durham,[53] who found that elongation can significantly enhance directional alignment and migration under shear. Interestingly, similar behaviors have been observed in studies of confined micro-swimmers, where anisotropic diffusion and external shear fields significantly alter migration patterns and orientation dynamics.[54] This structural rearrangement is associated with a decrease in shear stress and the elastic energy of the suspensions. Furthermore, it was demonstrated that the disorder-to-layered transformation is a shear-activated process. There is an initial induction period before the formation of the layered structure in which stress shows a pseudo-steady state behavior. This duration of this induction period follows a universal exponential decay as a function of shear rate with varying volume fractions. The same behavior was reported in large amplitude oscillatory shear flow when the maximum shear rate is large enough.[7]

As discussed, polydisperse concentrated suspensions show shear-induced phase transition in experiments and simulations.[15,45,55,56] On the other hand, bidispersity of particle size distribution has a notable impact on suspension rheology.[16,57,58] For example, a dense bidisperse suspension of

soft spheres exhibits a relative viscosity lower than that of a monodisperse hard-sphere suspension at the same hard particle volume fraction.[59] Previous work has verified the decrease in relative viscosity by experimentally studying bidisperse suspensions using non-Brownian glass beads in glycerin.[60] This difference in relative viscosity can be attributed to the capacity to attain a larger maximum packing fraction in soft colloidal suspensions.[61] In relation to our current study, Malbranche *et al.*[58] investigated the rheology of shear thickening bidisperse suspensions, and ordering was observed when the ratio of volume fraction of the large particles to total volume fraction was greater than 0.85. Inspired by this work, we investigate the rheology and microstructure of jammed suspensions formed by bidisperse soft particles. Specifically, our objectives are: (1) to understand the effect of the ratio of particle radii and their number density ratio on microstructure when bidisperse soft particles are considered, (2) to quantify the quality of the shear-induced phases using proper structural parameters such as in-plane pair distribution functions and bond order parameters and (3) to provide phase diagrams of bidisperse suspensions in shear flow. To pursue these objectives, we apply a three-dimensional (3D) particle simulations,[6] and explore the impact of particle size distribution, shear rate, and volume fraction on the evolution of microstructure in steady shear flow. Our results show that aside from volume fraction and shear rate, two additional parameters, which are the number density ratio of the large particles to small particles and the ratio of their radii, are needed to determine the shear-induced phase behavior. Tuning these parameters leads to the formation of shear-induced layered, amorphous, crystals and, in some rare cases, the coexistence between amorphous and ordered structures.

II. Simulation details and method

A. Suspensions specifications

$10,000$ particles with a bidisperse size distribution are suspended in a Newtonian liquid with a viscosity η_s in a cubic periodic box, as seen in Fig. 1(A). Two parameters are used to control the dispersity of the suspension, namely r and X. r represents the radius ratio of large to small particles, *i.e.*, $r = R_b/R_s$, and X represents the number density ratio of each population, *i.e.*, $X = n_b/n_s$. The volume fraction and the total number of particles are fixed; thus, the box length for a given volume fraction can vary by adjusting r and X values. Overall, three volume fractions, $\phi = 0.70, 0.80$, and 0.90, are studied in these simulations.

B. Force law and shear flow protocol

Following previous works on this topic,[1,6] we utilize the methodology for simulating SPGs in shear flow with a subtle difference in the force law where the normal contact elastic force ($\mathbf{f}^e_{\alpha\beta}$)

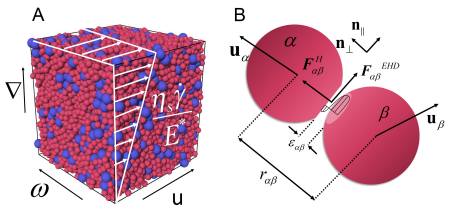

FIG. 1. (A) Configuration of a bidisperse suspension with a volume fraction of $\phi = 0.80$ with $X = 0.10$ and $r = 1.60$ subjected to shear flow with an applied shear rate of $\dot{\gamma}\eta_s/E^*$ in a periodic simulation box. The velocity ($\mathbf{u}$), gradient (∇), and vorticity (ω) directions are indicated. (B) Schematic showing the pair-wise interaction between particles α and β.

between particles are governed by the Hertz law according to:

$$\mathbf{f}^e_{\alpha\beta} = \frac{4}{3}E^*\varepsilon^{1.5}_{\alpha\beta}R^2_c\mathbf{n}_\perp, \tag{1}$$

where E^* is the contact modulus of the individual particle ($E^* = E/2(1-\nu^2)$, with E is the Young's modulus and ν is the Poisson ratio), $\varepsilon_{\alpha\beta}$ is the dimensionless overlap parameter which is defined as $\varepsilon_{\alpha\beta} = (R_\alpha + R_\beta - r_{\alpha\beta})/R_c$, where $R_c = R_\alpha R_\beta/(R_\alpha + R_\beta)$ is the effective radius of the two particles in contact and $r_{\alpha\beta}$ is the distance between particles α and β. $\mathbf{n}_\perp$ is the normal vector to the facets at contact as shown in Fig. 1(B). Two particles in contact also experience elastohydrodynamic ($\mathbf{f}^{EHD}_{\alpha\beta}$) force according to:

$$\mathbf{f}^{EHD}_{\alpha\beta} = -(\eta_s u_{\alpha\beta\parallel}E^*R^3_c)\varepsilon_{\alpha\beta}\mathbf{n}_\parallel, \tag{2}$$

where $u_{\alpha\beta\parallel}$ is the magnitude of the relative velocity of two particles in the direction parallel to the facets in contact, *i.e.*, $\mathbf{n}_\parallel$. The vector $\mathbf{n}_\parallel$ lies in the tangential plane at the contact point. Its specific direction within this plane is critical for modeling the sliding interactions that occur when particles move relative to each other under shear, and usually, this alignment is parallel to the shear direction, ensuring that the EHD force represents the shear-driven relative velocities of the particles along the contact plane. This particular orientation is necessary for calculating the component of relative velocity that is tangential to the point of contact, $\mathbf{u}^{rel}_{\mathbf{n}_\perp}$, which influences the shear interactions between the particles. It is calculated by $\mathbf{u}^{rel}_{\mathbf{n}_\perp} = (\mathbf{u}_\beta - \mathbf{u}_\alpha)\cdot\mathbf{n}_\perp\mathbf{n}_\perp = \mathbf{u}_{rel}\cdot\mathbf{n}_\perp\mathbf{n}_\perp$, where $\mathbf{u}^{rel}_{\mathbf{n}_\perp}$ is the component of relative velocity along $\mathbf{n}_\perp$. The relative tangential velocity is given by $\mathbf{u}^{rel}_{\mathbf{n}_\parallel} = \mathbf{u}_\parallel - (R_\alpha\boldsymbol{\Omega}_\alpha + R_\beta\boldsymbol{\Omega}_\beta)\times\mathbf{n}_\perp$, where $\mathbf{u}_\parallel = \mathbf{u}_r - \mathbf{u}_r\cdot\mathbf{n}_\perp\mathbf{n}_\perp$. In our suspensions, since the

volume fraction is high, the rotational motion of our particles is limited, therefore, $\mathbf{u}_{\mathbf{n}_\parallel}^{rel} = \mathbf{u}_\parallel$. The direction of the applied force is $\mathbf{n}_\parallel = \dfrac{\mathbf{u}_{\mathbf{n}_\parallel}^{rel}}{||\mathbf{u}_{\mathbf{n}_\parallel}^{rel}||}$. Considering these two forces and using the scales of the particle size R and time η_s/E^*, the dimensionless equation of motion for particle α in shear flow becomes:

$$\frac{d\tilde{\mathbf{x}}_\alpha}{d\tilde{t}} = \mathbf{u}_\alpha^\infty + \frac{\mathbf{M}}{\tilde{R}_\alpha} \cdot \left[\frac{4}{3} \left(\frac{\dot{\gamma}\eta_s}{E^*} \right)^{-1} \sum_\beta \varepsilon_{\alpha\beta}^{1.5} R_c^2 \mathbf{n}_\perp - \left(\frac{\dot{\gamma}\eta_s}{E^*} \right)^{-\frac{1}{2}} \sum_\beta \left(u_{\alpha\beta,\parallel} {R_c}^3 \right)^{\frac{1}{2}} \varepsilon_{\alpha\beta} \mathbf{n}_\parallel \right], \qquad (3)$$

where $\mathbf{M} = \frac{f(\phi)}{6\pi}\mathbf{I}$ ($\mathbf{I}$ is the identity tensor) is the mobility coefficient and is set to 0.01.[5] $\mathbf{u}_\alpha^\infty = \frac{\dot{\gamma}\eta_s}{E^*} y_\alpha \mathbf{e}_x$ describes the shear advection velocity of a particle α, $\mathbf{e}_x$ is the unit vector in the flow direction. Note that the dimensionless shear rate of $\dot{\gamma}\eta_s/E^*$ which emerges from this equation is used to impose the shear rate on the suspensions by applying the Lees–Edwards boundary conditions.[62] The stress tensor is then computed as a function of time using the Kirkwood formula, *i.e.*, $\boldsymbol{\sigma} = \frac{1}{L^3}\Sigma_\alpha \Sigma_\beta \mathbf{f}_{\alpha\beta}(\mathbf{x}_\alpha - \mathbf{x}_\beta)$, where $\mathbf{f}_{\alpha\beta}$ is the total force exerted on particle α by particle β, and L is the length of the cubic box.[63] In all simulations, the suspensions are subjected to shear flow for at least 200 strains.

III. Results and discussion

A. Shear rheology

The effects of particle radii ratio, r, and number density ratio, X, on shear stress, σ/E^*, and elastic energy, UR^3/E^*, per unit volume of suspensions as functions of strain, γ, at nondimensional shear rates of $\dot{\gamma}\eta_s/E^* = 10^{-4}$ (high) and $\dot{\gamma}\eta_s/E^* = 10^{-9}$ (low) are shown in Fig. 2. Starting from a disordered state, at a volume fraction of $\phi = 0.80$, the shear stress of suspensions with $r = 1.65$, $X = 0.50$ and $r = 1.65$, $X = 0.10$ shows an initial linear increase and an overshoot at $\gamma_p \cong 0.4$ (Fig. 2(A)). This overshoot strain is consistent with the range obtained for SPGs in previous simulations, $\gamma_p \cong 0.1 - 0.4$,[6] and experiments.[64] When $r = 1.65$, $X = 0.10$, the shear stress attains a steady state value after the overshoot point as seen in Fig. 2(A), when $r = 1.65$ and $X = 0.50$, the shear stress shows a pseudo-steady state over the strain of γ_{IND}, known as the induction period, before a rapid drop to its steady state value. The latter is reminiscent of the stress-strain behavior seen in polydisperse soft particles when the polydispersity index is smaller than 0.2. Over this strain interval, amorphous suspensions undergo structural rearrangements, which act as precursors to phase transition from glassy to layers parallel to the flow-vorticity plane[6,7] at larger strains. We also note that the trend of the γ_{IND} is similar to prior works;[6] γ_{IND} decreases with an increase in the shear rate and a decrease in the volume fraction.

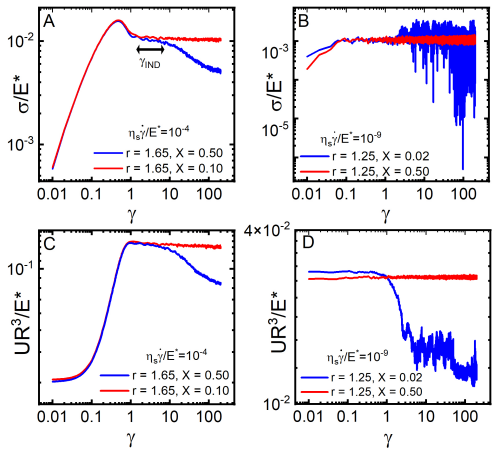

FIG. 2. (A and B) Shear stress, σ/E^*, and (C and D) elastic energy, UR^3/E^*, per unit volume as a function of shear strain, γ, for different bidisperse suspensions with $r = 1.65$, $X = 0.50$ and $X = 0.10$ at shear rate of $\dot{\gamma}\eta_s/E^* = 10^{-4}$, $r = 1.25$, $X = 0.02$ and $X = 0.50$ at shear rate of $\dot{\gamma}\eta_s/E^* = 10^{-9}$ at volume fraction of $\phi = 0.80$.

In Fig. 2(B), the stress response is plotted for the suspensions, which show glassy ($r = 1.25$, $X = 0.50$) and crystalline microstructures ($r = 1.25$, $X = 0.02$), at a low shear rate of $\dot{\gamma}\eta_s/E^* = 10^{-9}$. We note that we do not observe stress overshoot at low shear rates. The shear stress of the glassy microstructure reaches a steady state value after the initial increase. On the other hand, the system with $r = 1.25$, $X = 0.02$ enters a pseudo-steady state period before it shows fluctuations past a strain of $\gamma = 1$. The fluctuations in the stress values for the suspension are caused by the deviation of the particle's position from the lattice points, indicating the possibility of having a crystalline structure.[6] Similarly, the dimensionless elastic energy per unit volume shows the same behavior as observed in the shear stress (Fig. 2C-D). In suspensions under a high shear rate of $\dot{\gamma}\eta_s/E^* = 10^{-4}$, the elastic energy initially increases and then plateaus out for the glassy system, or decreases to its steady state for the layered configuration as shown in Fig. 2(C). The elastic energy shows constant values for the glassy structure while it rapidly drops at $\gamma = 1$ to its steady-state for the crystalline structure as shown in Fig. 2(D) at a low shear rate of $\dot{\gamma}\eta_s/E^* = 10^{-9}$.

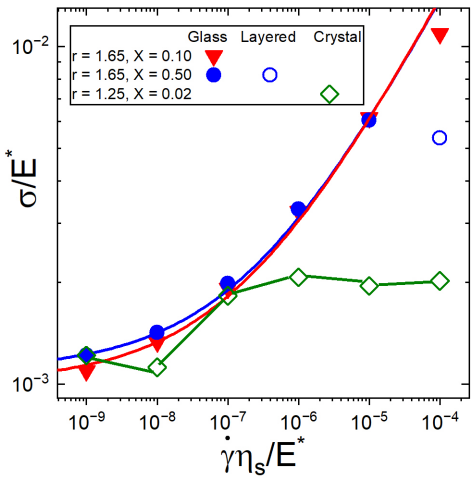

FIG. 3. Steady-state flow curve as a function of shear rate for suspensions with $r = 1.65, X = 0.10, 0.50$ and $r = 1.25, X = 0.02$ at volume fraction $\phi = 0.80$.

The flow curve of a few selected suspensions at $\phi = 0.80$, which cover a wide range of microstructures at steady-state, are presented in Fig. 3 (see Table. I for summary of results). The shear-stress response for the disordered suspensions with $r = 1.65, X = 0.10$ follows the HB equation. The exponent value obtained for the suspensions is $n = 0.4 \pm 0.05$, which is slightly smaller than the value of 0.5 found by SPGs with stiffer contact force law.[1,8] This deviation is also due to the limited number of shear rates investigated at higher rates. In addition, there is a weak dependence of the shear stress on the number density ratio of the suspensions, X, in the low shear rate regime. In contrast, the dependence of the flow curve on this parameter becomes negligible in the power-law flow regime. At high enough shear rates, *i.e.*, $\dot{\gamma}\eta_s/E^* = 10^{-4}$, the shear-stress response for the suspensions with $r = 1.65, X = 0.50$ plateaus instead of showing a monotonic increase. This behavior is a direct consequence of the decreases of the shear stress as seen in Fig. 2(A) where the stress attains a lower steady-state than the glassy suspensions after experiencing an induction period followed by crystallization. The discontinuity in the flow curve is similar to the results reported by Khabaz *et al.*[6,11] In suspensions with a low polydispersity index, a discontinuity in the flow curve at intermediate or high shear rates was observed for mildly polydisperse suspensions. This discontinuity shifts to higher shear rates when there is an increase in polydispersity and volume fraction of the suspensions. In the case of suspensions with $r = 1.25, X = 0.10$,

particles at all shear rates transition to ordered structures, but the nature of the microstructure shows a sharp change at a shear rate of $\dot{\gamma}\eta_s/E^* = 10^{-6}$ and then shear stress shows a significant drop than expected value based on the HB relationship. The rearrangements of particles occurring in the microstructure are responsible for the evolution in the shear stress and elastic energy seen in Fig. 2, which are discussed next.

TABLE I. Shear induced microstructures of the selected suspensions in III A.

Suspensions	**Shear rate** ($\dot{\gamma}\eta_s/E^*$)	**Microstructure**
$r = 1.65, X = 0.50$	10^{-4}	Layered
$r = 1.65, X = 0.10$	10^{-4}	Glassy
$r = 1.25, X = 0.02$	10^{-9}	Crystalline
$r = 1.25, X = 0.50$	10^{-9}	Glassy

B. Microstructure

1. Local microstructure

To clarify the effect of shear flow on the microstructure of suspensions at steady state, the two-dimensional (2D) pair distribution functions in the flow-gradient, $g_{u\nabla}(r)$, and flow-vorticity, $g_{u\omega}(r)$, planes are determined at different shear rates. Since there are two sets of particles, *i.e.*, small and large, all combinations of these pair distribution functions are determined in Figs. 4 and 5. At both high and low shear rates, $g_{u\nabla}(r)$ and $g_{u\omega}(r)$ for glassy structures show one major peak indicating that there is only a short range structure at contact distance between particles in the first neighbor shell. The latter confirms the existence of a disordered structure at steady state as shown in Figs. 4(A), 4(C), 5(B), and 5(D). However, when a layered microstructure is formed, more peaks are observed at large r, as seen in Figs. 4(B) and 4(D). Finally, crystalline structures show several well-defined peaks at large distances which are associated with the formation of an ordered phase (Figs. 5(C) and 5(A)). Comparison between the structures in the $u\omega$ and $u\nabla$ planes shows that there is a larger peak in the $g_{u\omega}(r)$ than in $g_{u\nabla}(r)$ which indicates that the particles are more packed in the flow-vorticity plane than the flow-gradient plane. The number density ratio and radius ratio of these bidisperse suspensions play a critical role in determining the final microstructure. Holding r constant and decreasing X results in a glassy microstructure, as seen in Fig. 4 and Fig. 5 while decreasing r and keeping X constant yield glassy and crystalline microstructures in selected systems. These variations indicate that different combinations of X

and r produce distinct microstructures and phase behaviors.

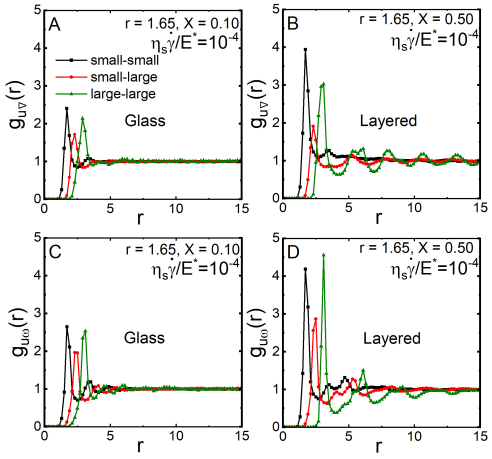

FIG. 4. Flow-gradient and flow-vorticity pair distribution functions of bidisperse suspensions at $\phi = 0.80$ as a function of the two-dimensional distance (r) at high shear rate of $\dot{\gamma}\eta_s/E^* = 10^{-4}$ and suspensions showing a glassy (A and C) and layered microstructure (B and D).

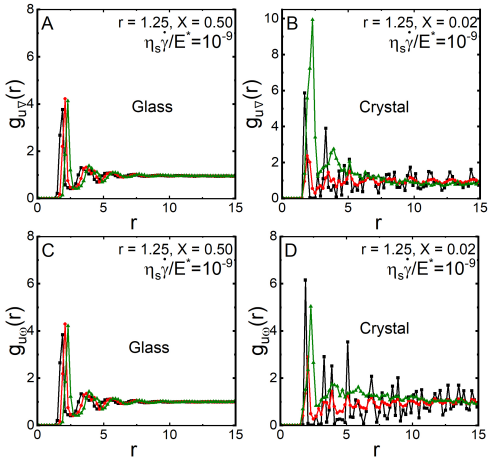

FIG. 5. Flow-gradient and flow-vorticity pair distribution functions of bidisperse suspensions at $\phi = 0.80$ as a function of the two-dimensional distance (r) at low shear rate of $\dot{\gamma}\eta_s/E^* = 10^{-9}$ and suspensions showing a glassy (A and C)and a crystalline (B and D) microstructure.

To measure the variance in the configuration of the particles at steady-state, especially the crystalline structures, the microstructures are characterized by calculating the local order parameters, q_l for particle i,[65–67] using the following equation:

$$q_l(i) = \sqrt{\frac{4\pi}{2l+1}\sum_{m=-l}^{l}\left|q_l^m(i)\right|^2}, \tag{4}$$

where l and m are indices used in the definition of spherical harmonics and, $q_l^m(i)$ is given as:

$$q_l^m(i) = \frac{1}{N_b(i)}\sum_{j=1}^{N_b(i)} Y_l^m(\mathbf{r}_{ij}), \tag{5}$$

$N_b(i)$ is the number of neighbors of particle i, $Y_l^m(\mathbf{r}_{ij})$ are spherical harmonics coefficients for neighboring particles j and $\mathbf{r}_{ij}$ is the separation vector. These parameters are quantitative metrics used to evaluate the level of order and arrangement within a set of particles and to detect whether the particles are in a fluid-like environment or a solid-like environment.[68] The q_l quantifies the degree of local ordering by assessing the symmetry and alignment of particles within a given region or cluster. This q_l parameter is close to zero in the amorphous phase and acquires a specific nonzero value for a given crystalline structure.[65] In our systems, we calculate these quantities for all particles. The probability density of q_l at the steady state, along with snapshots of the microstructure and analysis of crystalline structure, are presented for these selected systems in Fig. 6. A disordered microstructure can be seen in Fig. 6(A) for suspensions with $r = 1.65, X = 0.10$. In Fig. 6(B), when $r = 1.75, X = 0.8$, most of the particles are configured in layered structures parallel to the flow-vorticity plane that does not correspond to any known crystalline structures. Furthermore, Fig. 6(C) shows clusters of crystalline assemblies. Mostly FCC and HCP configurations are detected in the crystalline phase. The order parameters, q_4 and q_6 are particularly sensitive to the fourth and sixth orders of spherical harmonics, respectively. This makes them well-suited to detect symmetries associated with common crystal structures.[65] The distribution of q_4 and q_6 for glassy structure (Fig. 6D) shows normal distributions with average values of 0.1 and 0.2, respectively. These averages slightly shift to larger values for the layered structure (Fig. 6E). Interestingly, the distributions for the selected crystalline structure show a bimodal behavior with peak values of $q_4 = 0.169$ and 0.2, and $q_6 = 0.49$ and 0.538. Note that for a perfect FCC crystal lattice, values of $q_4 = 0.171$ and $q_6 = 0.507$ have been reported, whereas for a perfect HCP crystal, these parameters take values of $q_4 = 0.107$ and $q_6 = 0.445$, respectively.[65,69,70] In comparison to reported values, the co-existence of an FCC and an HCP crystalline structure is evident for $r = 1.25$ and $X = 0.02$.

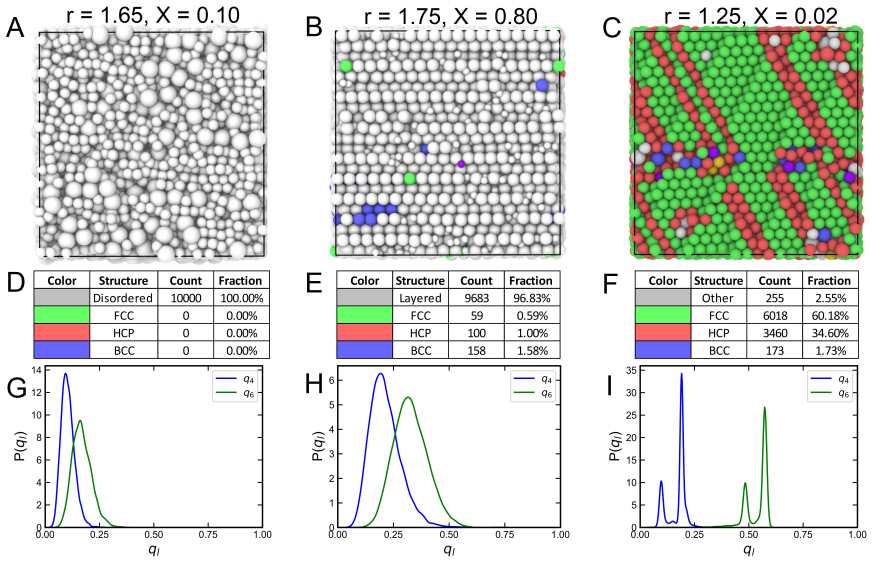

FIG. 6. (A-C) Microstructure, (D-F) crystallinity analysis, and (G-H) distribution of q_4 and q_6 values of suspensions with $r = 1.65, X = 0.10$, $r = 1.75, X = 0.80$, and $r = 1.25, X = 0.02$, at steady state. The crystalline phases have been identified using polyhedral template matching.[71]

In addition to the distribution of these parameters, average bond order parameters $\overline{q}_4$ and $\overline{q}_6$ are calculated and plotted as a function of strain, γ, in Fig. 7 at shear rates of $\dot{\gamma}\eta_s/E^* = 10^{-4}$ and 10^{-9}. These metrics provide a generalized view of the level of order within the system as the jammed suspensions are sheared. The results showed that the $\overline{q}_4$ and $\overline{q}_6$ values of the layered and crystalline bidisperse suspensions are higher than the glassy ones at both high and low shear rates. The $\overline{q}_4$ and $\overline{q}_6$ values of a layered system were higher than the glassy system, as shown in Fig. 7(A). In comparison between a glassy and a crystalline system, the crystalline system showed lower $\overline{q}_4$ but higher $\overline{q}_6$, indicating the prominent presence of an HCP crystal. Furthermore, the crystalline $\overline{q}_4$ and $\overline{q}_6$ values showed an initial increase until $\gamma \cong 10$ followed by fluctuations and attainment of a steady state as seen in Fig. 7(B).

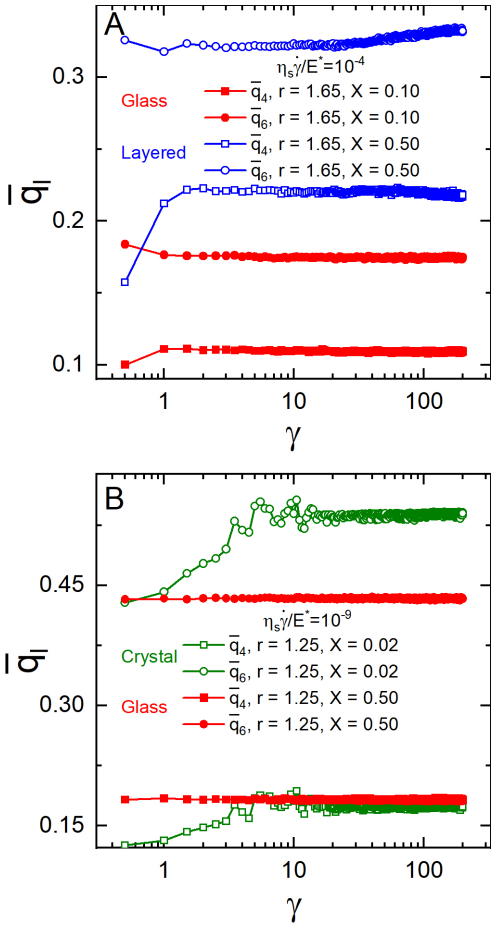

FIG. 7. Average bond order parameters ($\bar{q}_4$) and ($\bar{q}_6$) as a function of strain (γ) for different bidisperse systems at shear rates of (A) $\dot{\gamma}\eta_s/E^* = 10^{-4}$ and (B) $\dot{\gamma}\eta_s/E^* = 10^{-9}$. In each plot, two suspensions with ordered and disordered structures are selected.

2. *Phase diagram*

There are four parameters that control the phase behavior, *i.e.*, $\dot{\gamma}\eta_s/E^*$, X, r, and ϕ. Thus, considering the behavior of the pair distribution functions and using values of the local bond order parameters, q_4 and q_6,[6,7] we construct phase diagrams of these suspensions by holding the shear rate and volume fraction constant while varying X and r values as seen in Fig. 8. Depending

on the phase, q_4 and q_6 distribution can vary significantly. For an amorphous system, q_4 and q_6 values are 0.10 and a maximum of 0.36, respectively. The distribution is slightly shifted for layered structures, and the values do not fall under the amorphous criterion. Finally, in a HCP crystalline structure, the values of q_4 and q_6 are 0.107 and 0.445, respectively. These values are 0.17 and 0.507, respectively, for an FCC crystalline structure.[65,69,70] In addition to bond order parameters, polyhedral template matching[71] was used to identify if the particles correspond to any known crystalline configuration. If the majority of the particles (i.e., more than 90%) do not belong to any known lattice structure and form layers parallel to the flow-vorticity plane, they are called "layered," while others that show a coexistence between FCC and HCP are named crystal. Note that the layered systems show smooth steady stress response after the induction period, while crystals show high fluctuations. In Fig. 8(A-C), at high shear rates and a volume fraction of $\phi = 0.70$, only a small region with amorphous microstructure is present. This amorphous phase behavior is observed when $0.1 < X < 0.2$ and $1.6 < r < 1.75$. Outside of these domains, soft particles rearrange into either layered structures or form crystals in shear flow. With decreasing shear rate, the presence of glassy structures becomes more evident as seen in Fig. 8(D) and Fig. 8(E). Crystals start forming near monodisperse boundaries and when $X = 1$ at low shear rates of $\dot{\gamma}\eta_s/E^* = 10^{-8}$ and 10^{-9} as observed in Fig. 8(F). For $\phi = 0.80$, at high shear rates, crystals are observed at $X = 0.05$ and $X = 0.95$ for nearly all r considered. Fig. 8(G-L) shows that several glassy and crystalline phases are generated. When $r > 3$ and $X = 0.50$ crystals structures appear, and at $X = 0.95$, all systems at different particle size ratio r become crystal. This non-monotonic dependence of the phase diagram on the size ratio r, as observed in 8(E) can be attributed to a complex interplay of factors including particle size distribution, volume fraction, and shear-induced dynamics. In monodisperse systems, the uniformity of particle size promotes optimal packing under shear, facilitating the formation of crystalline structures. On the other hand, at very high size ratios, $r > 3$, the smaller particles can effectively fill the gaps between larger particles, enhancing order due to improved packing and alignment under shear. Moreover, the behavior under shear significantly influences the microstructural transitions from amorphous to ordered states, particularly noticeable at these size extremes. When size ratio, r, is large, the motion of small particles around larger ones under shear allows for more effective particle rearrangements, leading to crystalline formations.[72]

On the other hand, at $X = 0.05$, crystalline structures are seen only at $r < 2$. It can be concluded that at high shear rates, an increase in X and r will result in an ordered structure, and a decrease of

X towards a monodisperse system will result in crystallization. At lower shear rates, an increase in the dominance of the glassy phase is observed, accompanied by reduced layering and enhanced crystallization, as evident in Fig. 8(I) and Fig. 8(J). These results suggest the prevalence of the glassy phase and the suppression of layering in the majority of bidisperse suspensions, especially at the two lowest shear rates. Moving towards the lowest shear rates, crystals are formed, no layering occurs and the phases are glassy and crystalline as seen in Fig. 8(K) and Fig. 8(L). For the suspensions at $\phi = 0.90$, mostly glassy and crystalline structures are observed throughout the shear rates. Layering is only observed at the two highest shear rates of $\dot{\gamma}\eta_s/E^* = 10^{-4}$ and 10^{-5} and only glassy and crystalline structures are observed at lower shear rates.

Interestingly, at volume fractions of $\phi = 0.80$ and 0.90, a few suspensions, over the simulation time scale of 1000 strain units, show the coexistence of the amorphous and ordered structures. In these suspensions, large particles tend to form ordered structures, and the smaller ones form disordered microstructures (Fig.9). We note that the generic behavior of the flow curve and stress response of these systems with coexistence is similar to the ones forming layered structures. The pair distribution function between the small-small and large-large pairs confirms this existence. In summary, from the phase diagrams, it is observed that glassy systems are observed at low shear rates throughout all the volume fractions, layered microstructures are prevalent at high shear rates of $\dot{\gamma}\eta_s/E^* = 10^{-4}$ and 10^{-5}, especially at $\phi = 0.70$ and $\phi = 0.80$, and crystals are mostly found when suspensions compositions are close to a monodisperse case or large X values, where the number density ratio of the larger particles is greater.

C. Kinetics of the transition and reversibility

The shear stress and elastic energy in the bidisperse suspensions, which eventually transform into ordered structures, experience a swift decrease with strain after reaching the induction stage, where stress shows a relatively prolonged pseudo-steady behavior. As seen earlier, analysis of the microstructure revealed that this decline is associated with rearrangements in the structure within the flow-gradient and flow-vorticity planes. It was established that the γ_{IND} shows an exponential decay with the shear stress, *i.e.*, $\gamma_{IND} \sim \exp(-E/\sigma)$, where E is a fitting parameter.[6] Thus, the induction strain should decrease with the applied shear rate for a given suspension. Indeed, we also observe the same behavior for the bidisperse suspensions studied here in Fig. 10. As discussed earlier, there are four parameters that affect γ_{IND}, *i.e.*, $\gamma_{IND} = \gamma_{IND}(r, X, \dot{\gamma}\eta_s/E^*, \phi)$. Values of the induction strain γ_{IND} are plotted as a function of X and shear rate for systems with different volume fractions in Fig. 10. Throughout all volume fractions, the relationship between X and

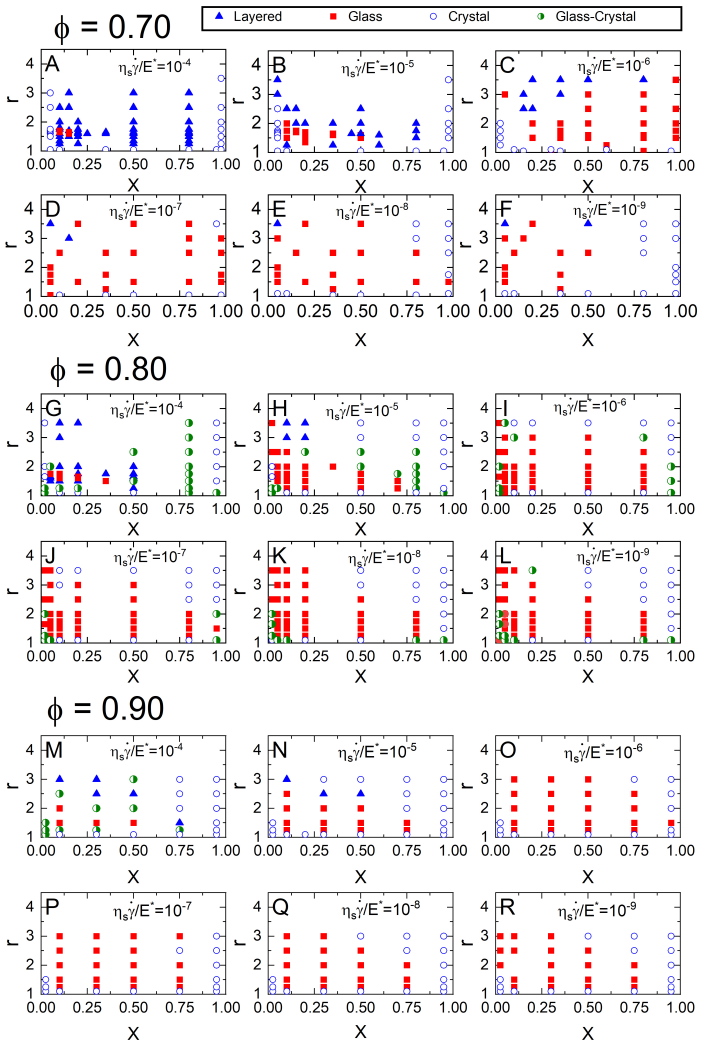

FIG. 8. Phase diagrams of the bidisperse SPGs as a function of number density ratio, X, and particle size ratio, r, at $\phi = 0.70$ (A-F), $\phi = 0.80$ (G-L), and $\phi = 0.90$ (M-R) at different shear rates ranging between $\dot{\gamma}\eta_s/E^* = 10^{-9}$ and 10^{-4}.

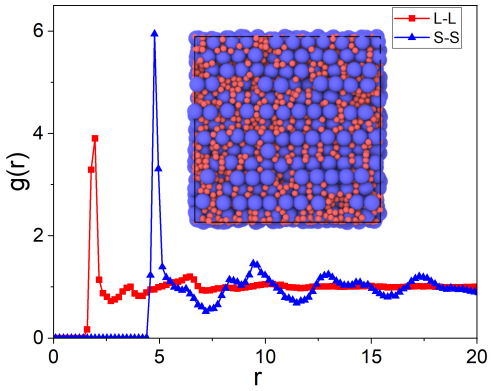

FIG. 9. 3D pair distribution function between liquid-liquid and solid-solid particles of suspensions with $r = 2.50$ and $X = 0.20$ at $\phi = 0.80$ and $\dot{\gamma}\eta_s/E^* = 10^{-5}$. Inset shows the flow-gradient view of the simulation box.

γ_{IND} is direct. γ_{IND} increases with an increase in number density ratio X and a decrease in shear rate $\dot{\gamma}\eta_s/E^*$. The longest induction stage of $\gamma_{IND} = 135$ was observed for a system with $\phi = 0.80$, $r = 3.50$, and $X = 0.95$ at shear rate of $\dot{\gamma}\eta_s/E^* = 10^{-6}$. However, there is no apparent correlation between r and the induction strain. Nevertheless, for a given r, the induction strain decreases with the increase of ϕ.

Furthermore, we track the evolution of the microstructure of selected systems as a function of strain for a selected system with $\phi = 0.80$ and $r = 2.00, X = 0.50$ in Fig. 11 by determining the maximum values of the 2D-dimensional pair distribution functions in both $u\nabla$ and $u\omega$ planes that correspond to their value at the first peak, whose location does not change as a function of strain. As shown on the graphs, the induction period for this system corresponds to the strain range of $1 < \gamma < 30$. During this period, the small-small and small-large pairs do not show a change in the value of $g^{max}_{u\nabla}(r)$. While $g^{max}_{u\omega}(r)$ shows a slight decrease between small-large and an increase for large-large pairs. Then, both the small-small (Fig. 11(A)) and large-large (Fig. 11(C)) pair distributions show transition increases with a high rate during the stress reduction stage. This increase is more pronounced for the large particles. After experiencing this transition, all pair distribution functions attain a steady state consistent with transient stress behavior. Note that in suspensions with low polydispersity index, particles showed rearrangement in the flow-vorticity plane during the induction period,[6] while in bidisperse suspensions, the majority of the structure

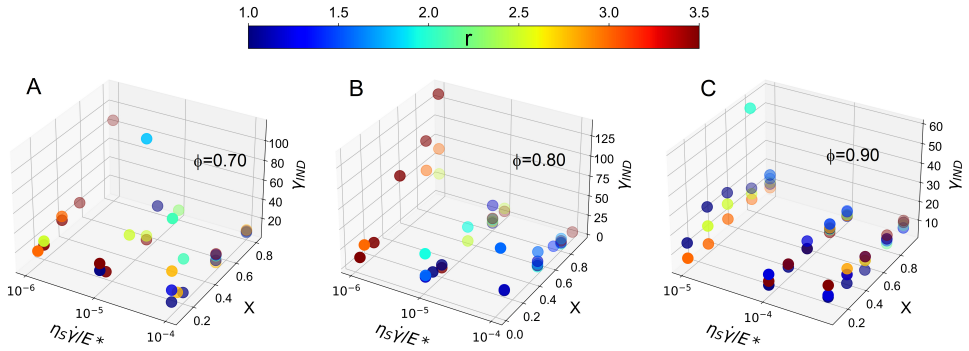

FIG. 10. Induction strain, γ_{IND}, as a function of the composition of the suspension, X, and shear rate, $\dot{\gamma}\eta_s/E^*$, obtained at (A) $\phi = 0.70$, (B) $\phi = 0.80$, and (C) $\phi = 0.90$. The color bar indicates the value of the particle size ratio, r.

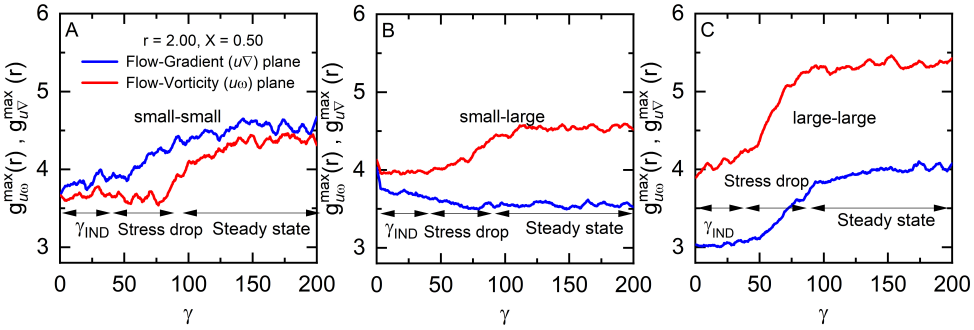

FIG. 11. The magnitude of the pair distribution function at the first peak between (A) small-small, (B) small-large, and (C) large-large pairs as a function of strain for a system with $\phi = 0.80$, $r = 2.00$, and $X = 0.50$ and at a shear rate of $\dot{\gamma}\eta_s/E^* = 10^{-5}$.

change occurs during the stress reduction stage.

We further test the reversibility of these transitions by subjecting the shear-induced structures to different shear rate rates. It is important to keep in mind that these phase transitions are shear-activated. For instance, as seen in Fig. 12 starting with a layered microstructure with $r = 2.00$ and $X = 0.5$ obtained at a shear rate of $\dot{\gamma}\eta_s/E^* = 10^{-5}$, the microstructure becomes amorphous as

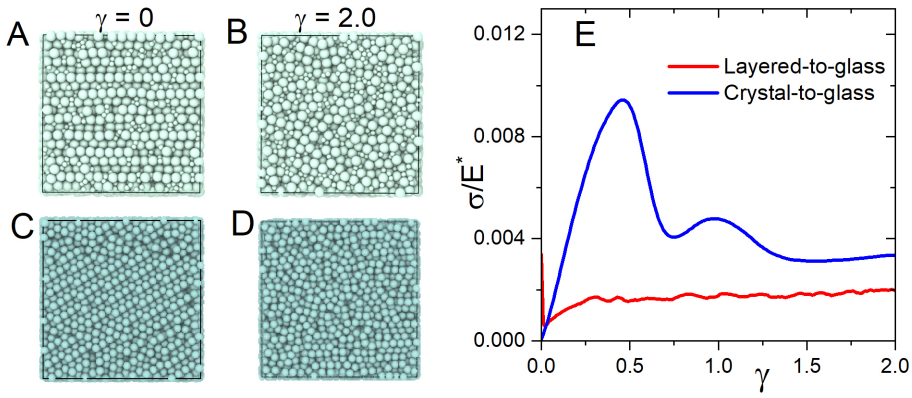

FIG. 12. Simulation snapshots of suspensions with (A and B) $r = 2.00$ and $X = 0.50$ and (C and D) $r = 1.05$ and $X = 0.95$ at $\gamma = 0$ and $\gamma = 2.0$. The shear rates used in these simulations are $\dot{\gamma}\eta_s/E^* = 10^{-6}$ and 10^{-5} for the layered and crystal phases, respectively. (E) Evolution of the shear stress as a function strain. The volume fraction of suspensions is $\phi = 0.80$.

the shear rate is decreased to $\dot{\gamma}\eta_s/E^* = 10^{-6}$. This observation is applicable to all layered structures. Consider a system with $r = 1.05$ and $X = 0.95$, the suspensions show crystalline structure at $\dot{\gamma}\eta_s/E^* = 10^{-9}$ as seen in Fig. 11(C-D). When this structure is subjected to a higher shear rate of $\dot{\gamma}\eta_s/E^* = 10^{-7}$ it transforms into an amorphous one. This behavior is reminiscent of the shear melting process seen in hard-sphere suspensions. Previous works[73,74] discovered that once a high shear rate is applied to an initially crystallized microstructure, the microstructure becomes disordered. Shear melting proceeds by temporary melting of localized domains of particles. With an increase in shear rate, particles spend more time in the disordered environments, but ordered domains keep nucleating and melting indefinitely, whereas the suspension as a whole is considered to be shear melted. In the case of soft particles, the critical strain required to eliminate the crystalline phase is about $\gamma \cong 0.5$. This is evident from the stress-strain curve shown in Fig. 12(E), where initially, stress linearly increases in the solid phase and reaches the static yield point, and then suspensions start flowing by significantly reducing the shear stress. Thus, this static yield strain highlights the end of the crystalline structure and the onset of the flow.

IV. Conclusions

We studied the effect of shear flow on the microstructure of jammed suspensions of bidisperse soft particles. Our results show that these soft jammed suspensions undergo shear-induced microstructural transformation depending on the applied shear rate, $\dot{\gamma}\eta_s/E^*$, and suspension volume fraction, ϕ, number density ratio of particles, X, and particle size ratio, r. Different combinations of X and r at a given volume fraction produce distinct microstructures such as crystal, amorphous, combination of crystal and amorphous, and layered phase. Typically, at high shear rates, the transient shear stress shows an overshoot and attains a steady state in amorphous suspensions, and their flow curve is described using the HB relationship. When shear-induced layering occurs, the shear stress shows a significant drop after experiencing an induction period and then reaches steady state. The duration of this induction period grows when shear rate increases and X decreases, though we observed no evident correlation between the induction strain and particle size ratio. The consequence of the latter is that flow curve plateaus in the suspensions showing layering.

These layers are formed in the direction parallel to the flow-vorticity plane. Analysis of the pair distribution function shows that during the induction period, there are minor structural rearrangements. The observed alignment and layered structuring in our bidisperse suspensions under shear bear similarities to the bioconvective patterns formed by gyrotactic cells in shear flows, highlighting the universal nature of shear-induced phenomena across different scales and systems.[75] The latter is somewhat different from our prior work,[6] where there were significant rearrangements for particles to form these layered structures. Clearly, when particles are bidisperse, the phase transition is facilitated. Furthermore, crystalline structures emerge when the suspensions are monodisperse or X is a large number. Bond order parameter analysis showed that these crystalline structures are dominated by HCP and FCC lattices. Apart from these distinct microstructures, a few suspensions showed a coexistence of the amorphous and crystals. In particular number and radius ratios, the larger particles formed the crystal domain, and the smaller ones showed an amorphous structure. Using these parameters along with the shear rate and volume fraction of the suspensions, shear-induced phase diagrams of these suspensions were constructed.

Examining the microstructure through pair distribution functions, bond order parameters, and phase diagrams provided further insights into the sensitivity of these jammed suspensions to variations in particle size distributions. The composition-dependent dominance of glassy, layered, or crystalline states showed the significance of r and X, especially in dictating the prevalence of spe-

cific structures at varying shear rates. In summary, this comprehensive study offers an understanding of the multifaceted interplay between parameters governing the microstructure and rheological responses of bidisperse suspensions of soft particles. The microstructures, which show coexistence between amorphous and crystal, persist over 1000 strain units and possibly correspond to a stable thermodynamic state rather than a kinetically trapped one. Furthermore, LaCour *et al.*[72] observed ordering in hard sphere suspensions when there is an excess of the smaller particles, where they act like plasticizers and enable suspensions to reach a greater supersaturation before kinetic arrest occurs. However, studying this phenomenon, *i.e.,* kinetic arrest, extends beyond the scope of the present study. This coexistence opens new avenues in shear-induced phase equilibrium problems in these suspensions which make a prominent distinction compared to the prior works. For example, a thermodynamic model based on the framework proposed by Bonnecaze *et al.*[76] may be utilized to describe this coexistence which will be pursued in future work. Bonnecaze *et al*.'s framework, which effectively utilizes excess entropy scaling to correlate transport properties such as viscosity and diffusivity with microstructural states, provides a robust basis for this analysis. By applying this model, we aim to determine whether the observed coexistent structures in our systems are thermodynamically stable or are results of kinetic entrapment. Finally, this research opens avenues to investigate the phase behavior of hard sphere suspensions with a bidisperse size distribution in shear flow since it has not been thoroughly investigated.

Data Availability Statement

Data are available upon reasonable request from the authors.

Conflicts of interest

The authors have no conflicts to disclose.

Author Contributions

Rakan Alrashdan: Conceptualization, investigation, visualization, formal analysis, Writing-first draft, Writing – review. Harry Kojo Yankah: Formal analysis and visualization. Michel Cloitre: Conceptualization, methodology, Writing – review & editing. Fardin Khabaz: Conceptualization, methodology, Writing – review & editing, funding acquisition, investigation, project administration.

Acknowledgment

RA, HKY, and FK gratefully acknowledge support from NSF grants CBET-2240760 and NRT-2152210.

References

[1]J. R. Seth, L. Mohan, C. Locatelli-Champagne, M. Cloitre, and R. T. Bonnecaze, "A micromechanical model to predict the flow of soft particle glasses," Nat. Mater **10**, 838–843 (2011).

[2]D. Vlassopoulos and M. Cloitre, "Tunable rheology of dense soft deformable colloids," Curr. Opin. Colloid Interface Sci. **19**, 561–574 (2014).

[3]E. Brown and H. M. Jaeger, "Shear thickening in concentrated suspensions: phenomenology, mechanisms and relations to jamming," Rep. Prog. Phys. **77**, 046602 (2014).

[4]E. Brown, H. Zhang, N. A. Forman, B. W. Maynor, D. E. Betts, J. M. DeSimone, and H. M. Jaeger, "Shear thickening and jamming in densely packed suspensions of different particle shapes," Phys. Rev. E **84**, 031408 (2011).

[5]T. Liu, F. Khabaz, R. T. Bonnecaze, and M. Cloitre, "On the universality of the flow properties of soft-particle glasses," Soft Matter **14**, 7064–7074 (2018).

[6]F. Khabaz, T. Liu, M. Cloitre, and R. T. Bonnecaze, "Shear-induced ordering and crystallization of jammed suspensions of soft particles glasses," Phys. Rev. Fluids **2**, 093301 (2017).

[7]F. Khabaz, M. Cloitre, and R. T. Bonnecaze, "Structural state diagram of concentrated suspensions of jammed soft particles in oscillatory shear flow," Phys. Rev. Fluids **3**, 033301 (2018).

[8]F. Khabaz, M. Cloitre, and R. T. Bonnecaze, "Particle dynamics predicts shear rheology of soft particle glasses," J. Rheol. **64**, 459–468 (2020).

[9]F. Khabaz, B. F. Di Dio, M. Cloitre, and R. T. Bonnecaze, "Transient dynamics of soft particle glasses in startup shear flow. part i: Microstructure and time scales," J. Rheol. **65**, 241–255 (2021).

[10]Y. Jiao, F. H. Stillinger, and S. Torquato, "Nonuniversality of density and disorder in jammed sphere packings," J. Appl. Phys. **109** (2011).

[11]F. Khabaz and R. T. Bonnecaze, "Thermodynamics of shear-induced phase transition of polydisperse soft particle glasses," Phys. Fluids **33** (2021).

[12]P. Sollich and N. B. Wilding, "Crystalline phases of polydisperse spheres," Phys. Rev. Lett. **104**, 118302 (2010).

[13]N. J. Wagner and J. F. Brady, "Shear thickening in colloidal dispersions," Phys. Today **62**, 27–32 (2009).

[14]M. Cloitre, R. Borrega, F. Monti, and L. Leibler, "Glassy dynamics and flow properties of soft colloidal pastes," Phys. Rev. Lett. **90**, 068303 (2003).

[15]P. Pusey, E. Zaccarelli, C. Valeriani, E. Sanz, W. C. Poon, and M. E. Cates, "Hard spheres: crystallization and glass formation," Philos. Trans. R. Soc., A **367**, 4993–5011 (2009).

[16]P. Maßhoff, I. Elsner, M. Escobedo-Sánchez, J. Segovia-Gutiérrez, A. Pamvouxoglou, and S. Egelhaaf, "Shear-induced crystallisation in binary colloidal suspensions investigated using confocal microscopy," J. Phys.: Mater. **3**, 035004 (2020).

[17]S. Lopez-Godoy, P. Díaz-Leyva, and A. Kozina, "Self-assembly in binary mixtures of spherical colloids," Adv. Colloid Interface Sci. **308**, 102748 (2022).

[18]A. B. Schofield, P. Pusey, and P. Radcliffe, "Stability of the binary colloidal crystals a b 2 and a b 13," Phys. Rev. E **72**, 031407 (2005).

[19]P. Francis, S. Martin, G. Bryant, W. Van Megen, and P. Wilksch, "A bragg scattering spectrometer for studying crystallization of colloidal suspensions," Rev. Sci. Instrum. **73**, 3878–3884 (2002).

[20]W. Van Megen, V. Martinez, and G. Bryant, "Scaling of the space-time correlation function of particle currents in a suspension of hard-sphere-like particles: exposing when the motion of particles is brownian," Phys. Rev. Lett. **103**, 258302 (2009).

[21]S. Martin, G. Bryant, and W. Van Megen, "Observation of a smecticlike crystalline structure in polydisperse colloids," Phys. Rev. Lett. **90**, 255702 (2003).

[22]S. Martin, G. Bryant, and W. Van Megen, "Crystallization kinetics of polydisperse colloidal hard spheres: Experimental evidence for local fractionation," Phys. Rev. E **67**, 061405 (2003).

[23]H. J. Schöpe, G. Bryant, and W. Van Megen, "Two-step crystallization kinetics in colloidal hard-sphere systems," Phys. Rev. Lett. **96**, 175701 (2006).

[24]H. J. Schöpe, G. Bryant, and W. Van Megen, "Small changes in particle-size distribution dramatically delay and enhance nucleation in hard sphere colloidal suspensions," Phys. Rev. E **74**, 060401 (2006).

[25]G. Ovarlez and E. Guazzelli, "Shear-induced migration of rigid spheres in a couette flow," (2024), submitted.

[26]S. Sun, N. Xue, S. Aime, H. Kim, J. Tang, G. H. McKinley, H. A. Stone, and D. A. Weitz, "Anomalous crystalline ordering of particles in a viscoelastic fluid under high shear," Proc. Natl. Acad. Sci. **120**, e2304272120 (2023).

[27]C.-T. Liao, Y.-F. Wu, W. Chien, J.-R. Huang, and Y.-L. Chen, "Modeling shear-induced particle ordering and deformation in a dense soft particle suspension," J. Phys.: Condens.Matter **29**, 435101 (2017).

[28]K. Galloway, E. Teich, X. Ma, C. Kammer, I. Graham, N. Keim, C. Reina, D. Jerolmack, A. Yodh, and P. Arratia, "Relationships between structure, memory and flow in sheared disordered materials," Nat. Phys. **18**, 565–570 (2022).

[29]S. Paulin, B. J. Ackerson, and M. Wolfe, "Equilibrium and shear induced nonequilibrium phase behavior of pmma microgel spheres," J. Colloid Interface Sci. **178**, 251–262 (1996).

[30]H. Senff and W. Richtering, "Temperature sensitive microgel suspensions: Colloidal phase behavior and rheology of soft spheres," J. Chem. Phys. **111**, 1705–1711 (1999).

[31]J. J. Crassous, M. Siebenbürger, M. Ballauff, M. Drechsler, O. Henrich, and M. Fuchs, "Thermosensitive core-shell particles as model systems for studying the flow behavior of concentrated colloidal dispersions," J.Chem. Phys. **125** (2006).

[32]D. Paloli, P. S. Mohanty, J. J. Crassous, E. Zaccarelli, and P. Schurtenberger, "Fluid–solid transitions in soft-repulsive colloids," Soft Matter **9**, 3000–3004 (2013).

[33]B. Sierra-Martin and A. Fernandez-Nieves, "Phase and non-equilibrium behaviour of microgel suspensions as a function of particle stiffness," Soft Matter **8**, 4141–4150 (2012).

[34]C. N. Likos, "Effective interactions in soft condensed matter physics," Physics Reports **348**, 267–439 (2001).

[35]P. N. Pusey and W. Van Megen, "Phase behaviour of concentrated suspensions of nearly hard colloidal spheres," Nature **320**, 340–342 (1986).

[36]E. Zaccarelli and W. C. Poon, "Colloidal glasses and gels: The interplay of bonding and caging," Proceedings of the National Academy of Sciences **106**, 15203–15208 (2009).

[37]H. He, J. Lee, Z. Jiang, Q. He, J. Dinic, W. Chen, S. Narayanan, and X.-M. Lin, "Kinetics of shear-induced structural ordering in dense colloids," J. Phys. Chem. B **127**, 7408–7415 (2023).

[38]B. J. Ackerson, "Shear induced order and shear processing of model hard sphere suspensions," J. Rheol. **34**, 553–590 (1990).

[39]T. Besseling, M. Hermes, A. Fortini, M. Dijkstra, A. Imhof, and A. Van Blaaderen, "Oscillatory shear-induced 3d crystalline order in colloidal hard-sphere fluids," Soft Matter **8**, 6931–6939 (2012).

[40]J. Zhang, P. M. Lettinga, J. K. Dhont, and E. Stiakakis, "Direct visualization of conformation and dense packing of dna-based soft colloids," Phys. Rev. Lett. **113**, 268303 (2014).

[41]W. Pan, B. Caswell, and G. E. Karniadakis, "Rheology, microstructure and migration in brownian colloidal suspensions," Langmuir **26**, 133–142 (2010).

[42]A. Scotti, M. F. Schulte, C. G. Lopez, J. J. Crassous, S. Bochenek, and W. Richtering, "How softness matters in soft nanogels and nanogel assemblies," Chem. Rev. **122**, 11675–11700 (2022).

[43]S. Franco, E. Buratti, V. Nigro, E. Zaccarelli, B. Ruzicka, and R. Angelini, "Glass and jamming rheology in soft particles made of pnipam and polyacrylic acid," Int. J. Mol. Sci. **22**, 4032 (2021).

[44]T. Eckert and W. Richtering, "Thermodynamic and hydrodynamic interaction in concentrated microgel suspensions: Hard or soft sphere behavior?" J. Chem. Phys. **129** (2008).

[45]A. Scotti, U. Gasser, E. Herman, J. Han, A. Menzel, L. A. Lyon, and A. Fernandez-Nieves, "Phase behavior of binary and polydisperse suspensions of compressible microgels controlled by selective particle deswelling," Phys. Rev. E **96**, 032609 (2017).

[46]J. D. Olarte-Plata, G. Brekke-Svaland, and F. Bresme, "The influence of surface roughness on the adhesive interactions and phase behavior of suspensions of calcite nanoparticles," Nanoscale **12**, 11165–11173 (2020).

[47]N. Cuny, E. Bertin, and R. Mari, "Dynamics of microstructure anisotropy and rheology of soft jammed suspensions," Soft Matter **18**, 328–339 (2022).

[48]J. D. Park and S. A. Rogers, "Rheological manifestation of microstructural change of colloidal gel under oscillatory shear flow," Phys. Fluids **32** (2020).

[49]B. K. Ryu, S. M. Fenton, T. T. Nguyen, M. E. Helgeson, and R. N. Zia, "Modeling colloidal interactions that predict equilibrium and non-equilibrium states," J. Chem. Phys. **156** (2022).

[50]J.-R. Huang and T. G. Mason, "Deformation, restructuring, and un-jamming of concentrated droplets in large-amplitude oscillatory shear flows," Soft Matter **5**, 2208–2214 (2009).

[51]J. Ruiz-Franco, J. Marakis, N. Gnan, J. Kohlbrecher, M. Gauthier, M. Lettinga, D. Vlassopoulos, and E. Zaccarelli, "Crystal-to-crystal transition of ultrasoft colloids under shear," Phys. Rev. Lett. **120**, 078003 (2018).

[52]J. Vermant and M. J. Solomon, "Flow-induced structure in colloidal suspensions," J. Phys.: Condens.Matter **17**, R187 (2005).

[53]R. Bearon and W. Durham, "Elongation enhances migration through hydrodynamic shear," Phys. Rev. Fluids **8**, 033101 (2023).

[54]V. A. Shaik, Z. Peng, J. F. Brady, and G. J. Elfring, "Confined active matter in external fields," Soft Matter **19**, 1384–1392 (2023).

[55]Y. He, B. J. Ackerson, W. van Megen, S. M. Underwood, and K. Schätzel, "Dynamics of crystallization in hard-sphere suspensions," Phys. Rev. E **54**, 5286 (1996).

[56]R. A. Lionberger and W. Russel, "Microscopic theories of the rheology of stable colloidal dispersions," Adv. Chem. Phys. **111**, 399–474 (2000).

[57]A. Poslinski, M. Ryan, R. Gupta, S. Seshadri, and F. Frechette, "Rheological behavior of filled polymeric systems ii. the effect of a bimodal size distribution of particulates," J. Rheol. **32**, 751–771 (1988).

[58]N. Malbranche, B. Chakraborty, and J. F. Morris, "Shear thickening in dense bidisperse suspensions," J. Rheol. **67**, 91–104 (2023).

[59]S. Pednekar, J. Chun, and J. F. Morris, "Bidisperse and polydisperse suspension rheology at large solid fraction," J. Rheol. **62**, 513–526 (2018).

[60]A. P. Shapiro and R. F. Probstein, "Random packings of spheres and fluidity limits of monodisperse and bidisperse suspensions," Phys. Rev. Lett. **68**, 1422 (1992).

[61]J. Chong, E. Christiansen, and A. Baer, "Rheology of concentrated suspensions," J. Appl. Polym. Sci. **15**, 2007–2021 (1971).

[62]A. Lees and S. Edwards, "The computer study of transport processes under extreme conditions," J. Phys. C: Solid State Phys. **5**, 1921 (1972).

[63]R. G. Larson, *The structure and rheology of complex fluids* (Oxford University Press, New York, USA, 1999).

[64]B. F. Di Dio, F. Khabaz, R. T. Bonnecaze, and M. Cloitre, "Transient dynamics of soft particle glasses in startup shear flow. part ii: Memory and aging," J. Rheol. **66**, 717–730 (2022).

[65]P. J. Steinhardt, D. R. Nelson, and M. Ronchetti, "Bond-orientational order in liquids and glasses," Phys. Rev. B **28**, 784 (1983).

[66]Y. Wang, S. Teitel, and C. Dellago, "Melting of icosahedral gold nanoclusters from molecular dynamics simulations," J. Chem. Phys. **122** (2005).

[67]N. Duff and D. J. Lacks, "Shear-induced crystallization in jammed systems," Phys. Rev. E **75**, 031501 (2007).

[68]P. K. Bommineni, M. Klement, and M. Engel, "Spontaneous crystallization in systems of binary hard sphere colloids," Phys. Rev. Lett. **124**, 218003 (2020).

[69]W. Lechner and C. Dellago, "Accurate determination of crystal structures based on averaged local bond order parameters," J. Chem. Phys. **129** (2008).

[70]H. Eslami, P. Sedaghat, and F. Müller-Plathe, "Local bond order parameters for accurate determination of crystal structures in two and three dimensions," Phys. Chem. Chem. Phys. **20**, 27059–27068 (2018).

[71]P. M. Larsen, S. Schmidt, and J. Schiøtz, "Robust structural identification via polyhedral template matching," Modell. Simul. Mater. Sci. Eng. **24**, 055007 (2016).

[72]R. A. LaCour, T. C. Moore, and S. C. Glotzer, "Tuning stoichiometry to promote formation of binary colloidal superlattices," Phys. Rev. Lett. **128**, 188001 (2022).

[73]Y. L. Wu, D. Derks, A. van Blaaderen, and A. Imhof, "Melting and crystallization of colloidal hard-sphere suspensions under shear," Proc. Natl. Acad. Sci. **106**, 10564–10569 (2009).

[74]M. E. Helgeson, N. J. Wagner, and D. Vlassopoulos, "Viscoelasticity and shear melting of colloidal star polymer glasses," J. Rheol. **51**, 297–316 (2007).

[75]Y. Hwang and T. Pedley, "Bioconvection under uniform shear: linear stability analysis," J. Fluid Mech. **738**, 522–562 (2014).

[76]R. T. Bonnecaze, F. Khabaz, L. Mohan, and M. Cloitre, "Excess entropy scaling for soft particle glasses," J. Rheol. **64**, 423–431 (2020).